J Mater Sci (2013) 48:5880–5898
DOI 10.1007/s10853-013-7384-8

Microstructural evolution in two alkali multicomponent silicate glasses as a result of long-term exposure to solid oxide fuel cell environments

Amit Shyam · Rosa Trejo · Dana McClurg · Alexander Ladouceur · Melanie Kirkham · Xueyan Song · Jane Howe · Edgar Lara-Curzio

Received: 7 December 2012 / Accepted: 12 April 2013 / Published online: 23 April 2013

Abstract The microstructural evolution in two potential solid oxide fuel cell (SOFC) sealing glass materials exposed to air and a gas mixture of steam + H_2 + N_2 at 800 °C up to 10000 h was determined. The glass exposures were performed on common SOFC substrates like alumina and zirconia. Characterization of the crystalline phases and pore size distribution was performed for the specimens with various exposure conditions. Comparison of the microstructural and chemical stability of the two glasses was performed based on known trends related to glass chemistry. It was observed that multicomponent glasses followed few rules for chemical and microstructural stability reported in the literature for glasses with fewer components. The two glasses examined in this study displayed adequate resistance to devitrification but marginal resistance to porosity changes in the SOFC environment exposure. The implications of the results for the design and long-term performance of SOFC seals are discussed.

Introduction

Solid oxide fuel cells (SOFCs) are clean technological devices that convert the chemical energy stored in fuels into electric power [1]. SOFCs are fuel flexible and can generate power from gasified coal. SOFC technology is cost-effective with high energy conversion efficiency and can be applied for carbon capture and sequestration. Planar stack SOFCs are being pursued due to the higher power density associated with this design [2]. The planar stack designs, however, require seals to prevent the intermixing of gases. Seals must operate under demanding conditions (temperature ~800 °C, oxidizing and reducing environments) by meeting thermal, physical, chemical, mechanical and electrical property requirements for up to 40000 h while maintaining their functional, that is, sealing properties [3–5]. The development of low-cost reliable seals that can meet the aforementioned requirements of SOFCs is one of the main technological hurdles for the widespread commercialization of planar solid oxide fuel cells.

Typical seal designs include glass-ceramic materials that provide a rigid bond between components being sealed [6, 7]. More recently, compliant glass seal designs have been developed where the sealing temperature is typically above the glass softening temperature [8, 9]. The advantages of incorporating compliant seal materials are that the thermal stresses in the seal and adjacent components are relieved at temperatures above the glass transition temperature and that cracks that might form during cooling can be healed during subsequent heating.

The desired initial property requirements for sealing, for example, the coefficient of thermal expansion, glass transition temperature and wetting characteristics, have been achieved for several sealing architectures. As a recent review paper [4] concluded, the long-term stability of glass seal materials has been a persistent problem. Here, we report the effect of long-term exposure on phase stability and chemical compatibility of two commercially available multicomponent silicate glasses with potential use for SOFC sealing. The microstructural evolution including the

A. Shyam (✉) · R. Trejo · D. McClurg · A. Ladouceur · M. Kirkham · J. Howe · E. Lara-Curzio
Materials Science and Technology Division, Oak Ridge National Laboratory, 1 Bethel Valley Road, Oak Ridge, TN 37831-6069, USA
e-mail: shyama@ornl.gov

X. Song
Mechanical and Aerospace Engineering, West Virginia University, Morgantown, WV 26506, USA

precipitation of crystalline phases and evolution of porosity was characterized for up to 10000 h of exposure to air and a gas mixture consisting of steam + H_2 + N_2. The initial mechanical properties and sealing characteristics of these glasses have already been reported [9–11]. The implications of the evolution of the microstructure, phase stability and chemical compatibility on the functional characteristics of these glasses, exposed on SOFC substrates, will be discussed. Zirconia and alumina were chosen as the SOFC support substrates. Zirconia-based compositions are commonly applied as SOFC electrolytes, whereas both zirconia and alumina coatings are applied over ferritic stainless steel interconnects [11, 12].

Materials and experimental procedure

Materials

Two commercial glasses were evaluated: SCN glass (SEM-COM Co. Inc., Toledo, OH 43623, USA) and G6 glass (Whatman Ltd., Piscataway, NJ 08855, USA). The oxide composition of the two glasses determined by inductively coupled plasma acoustic emission spectroscopy (ICPAES) is presented in Table 1. Details of these compositional studies were reported elsewhere [10]. Barring silicon and oxygen, SCN glass had the following major elements in decreasing concentration: K > Ba > Na > Ca > Al > Mg > Ti. Although the silicon concentration in G6 was similar to SCN, the corresponding elements present in decreasing concentration were: Na > Ba > B > Zn > Al > Ca > K > Mg. Oxides that are detected in compositions <0.1 mol% are not listed in Table 1. The major constituents in both glasses are alkali and alkaline earth elements. G6 contains 9.5 mol% B_2O_3, which is not present in SCN.

Table 1 Oxide composition of SCN and G6 glass based on inductively coupled acoustic emission spectroscopy (ICPAES)

Oxide	SCN (mol%)	G6 (mol%)
SiO_2	73.6	65.3
K_2O	6.5	1.4
BaO	3.5	1.8
Na_2O	6.8	9.3
CaO	4.7	4.3
Al_2O_3	2.4	3.2
MgO	2.0	2.2
TiO_2	0.5	–
B_2O_3	–	9.5
ZnO	–	3.0

Specimen preparation for environmental exposure

SCN glass was obtained in powder form (average particle size ~10 μm), whereas G6 glass was acquired in the form of a planar mat of thickness 200 μm consisting of glass fibers bonded with an organic binder. The SCN glass powder was cold-pressed into either cylindrical (~10 mm diameter) or rectangular (25 mm × 37.5 mm) pellets with high-strength stainless steel dies. 8-mm-diameter disks were punched out of G6 glass mats and stacked (total 50 disks) prior to sintering. The sintering of both glasses was performed on dense 8YSZ (Fuel Cell Materials, Lewis Center, OH 43035, USA) or alumina (CoorsTek, Golden, CO 80403, USA) substrates by exposing the substrate + glass specimen in a furnace at 850 °C for 2 h with heating and cooling rates of 3 °C/min. The characteristics of the 8YSZ and alumina substrates including their surface finish are listed in Table 2. The initial roughness of the substrates was measured by a non-contact laser profilometer (Rodenstock, Columbus, OH 43212, USA). The sintered pellets and stacked disks adopted a bead shape after sintering [10].

Environmental exposure and specimen extraction schedule

Sintered G6 and SCN glass specimens on alumina/8YSZ substrates were exposed to air or a gas environment consisting of steam + H_2 + N_2. The exposure temperature was set to be 800 °C for both exposure environments, which is close to the average operating temperature of intermediate temperature SOFCs. Exposures to air environment were performed in a static environment in a box furnace. Exposures to gas mixtures of steam + H_2 + N_2 were performed in a tubular furnace with a constant flow rate. This gas mixture was obtained by spraying distilled water, using a pneumatic pump, to a gas stream consisting of 15 % H_2 and 85 % N_2. The amount of water added to the mixture was 38 % by volume. The exposure gas mixture therefore had the following composition by volume: water vapor, 38 %; hydrogen, 9 %; and nitrogen, 53 %. The experimental setup consisted of a three-zone horizontal furnace with a 3.5-inch-inner-diameter alumina tube and metal end caps with ports for gas inlets and outlets.

Table 2 Characteristics of the substrates for glass sintering and subsequent environmental exposure

Substrate	Vendor	Roughness (R_a, μm)	Thickness (mm)
8YSZ	Fuel cell materials	0.525	0.30
Al_2O_3	CoorsTek	0.106	0.75

To avoid water condensation outside the furnace, portions of the alumina tube outside the furnace as well as the metallic end caps were wrapped with heating tape. In addition to the furnace thermocouples, two thermocouples were placed near each end cap to control the temperature of the heating tapes at ~200 °C. The heating tape ensured that the water added to the gas mixture of hydrogen and nitrogen did not condense until it exited the sealed reservoir, where it was collected as liquid water. The collected liquid water at the outlet port was measured to further verify the water vapor content of the gas mixture.

The specimens were exposed for a long term on an alumina tray with several specimens exposed simultaneously. The exposure tests were interrupted periodically, and selected specimens were removed for non-destructive characterization and less frequently for destructive characterization. Non-destructive characterization consisted of surface scanning electron microscopy (SEM) including energy-dispersive spectroscopy (EDS). In addition, X-ray diffraction (XRD) was performed on the bead + substrate system to identify the crystalline phases that form on the surface of the specimen. The non-destructive characterization of specimens was performed approximately every 1000 h.

The cross sections of test specimens were examined after 100, 500, 850, 5000 and 10000 h of exposure by slicing specimens in half with a diamond wheel after embedding the exposed specimen in epoxy. Embedding the sample in epoxy was necessary to prevent damaging the specimen during slicing. One half of the specimen was metallographically prepared for cross-sectional examination of the morphology and chemistry of the crystalline phases and porosity. The interfacial region between the glass and the substrate was examined by both SEM and high-resolution transmission electron microscopy (HRTEM). The other half of the glass bead was manually detached from the substrate and pulverized prior to XRD analysis for identification of the major phases in the bulk of the glass specimen.

As-sintered and exposed glass characterization

As-sintered and exposed G6 and SCN glass specimens were characterized for surface and bulk phase evolution and interfacial reactivity with 8YSZ or alumina by applying a suite of characterization techniques. The surface and cross section regions were characterized in an SEM (Hitachi S3400) with an EDS detector. Elemental maps were collected using energy-dispersive spectroscopy. Extensive SEM study was carried out to understand the formation, morphology and evolution of crystalline phases and porosity in the cross section. X-ray diffraction (XRD) was performed in a PANalytical X'Pert Pro diffractometer with Cu Kα radiation. Transmission electron microscopy (TEM) was undertaken in selected specimens to examine the microstructure of the interface between the glass and substrate. Some TEM samples from the interfacial regions were prepared by the "lift-out" focused ion beam (FIB) technique using a Hitachi NB-5000 FIB-SEM system. Other TEM samples were prepared by mechanical polishing and ion milling in a liquid-nitrogen-cooled holder. The TEM imaging and analysis were performed using a Hitachi HF-3300 TEM/STEM operated at 300 kV and a JEM-2100 operated at 200 kV. A schematic summarizing the procedure used for microstructure evolution characterization is presented in Fig. 1. Mass of the glass bead + substrate specimen was measured before and after each exposure.

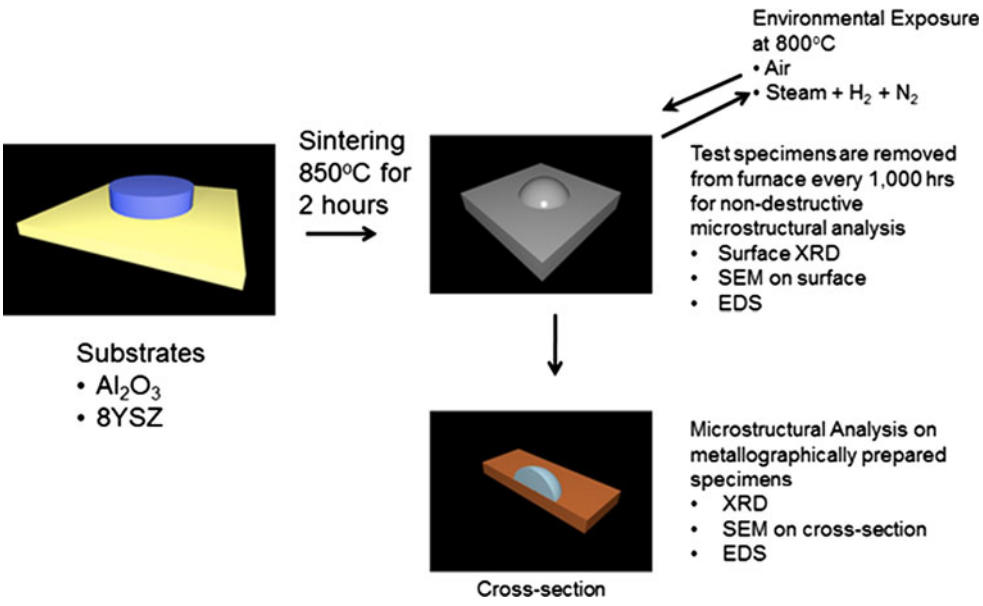

Fig. 1 A schematic depicting the procedure used for environmental exposure and subsequent characterization of as-sintered and exposed SCN and G6 glass specimens on 8YSZ/alumina substrates

Assuming the substrate does not change mass with exposure, the change in mass of the bead + substrate specimen was attributed to the volatility of species in the glass.

SCN glass microstructural evolution

Analysis assumptions

As mentioned above, glass/ceramic substrate specimens were placed in two different environments for different times of exposure. In subsequent sections, we analyze the microstructure of test specimens to assess the effect of environment and time of exposure. The implicit assumption in the following discussions is that all the specimens were statistically similar after cold-pressing and sintering. In other words, initial differences between specimens, if present, have not been taken into consideration. For example, it is assumed that all specimens have identical initial pore size distributions after sintering, so any changes in the pore size distribution after exposure will be attributed to physical mechanisms attributed to the exposure conditions. In this section, we discuss the microstructural evolution in SCN glass, and in section "G6 glass microstructural evolution", we discuss the corresponding changes in the microstructure of G6 glass as a result of environmental exposure.

SCN glass microstructure evolution on 8YSZ substrate

The effect of exposure to two environments, namely air and steam + H_2 + N_2, on the microstructural changes in SCN glass is summarized in this section. For brevity, when the effect of the two environments on microstructural changes in SCN glass is similar; results from only one of the two are shown. The effect of the steam + H_2 + N_2 environment exposure on SCN glass dimensional stability on an 8YSZ substrate is illustrated in Fig. 2. The metallographically prepared cross sections in Fig. 2 suggest that glass continues to flow under the influence of gravitational forces during the high-temperature exposure. This is evidenced by a decrease in the contact angle between the glass and the 8YSZ substrate from 85°, for the as-sintered specimen, to 14° after 10000 h of exposure.

The effect of air exposure on the microstructure of glass is shown at higher magnification in a series of micrographs in Fig. 3. Figure 3 illustrates the following major microstructural changes in SCN glass due to environmental exposure:

- A fine distribution of pores coalesces into a smaller number of larger pores.
- While the as-sintered glass was completely amorphous, a fine homogeneous distribution of precipitates appears after 100 h of air exposure and continues to grow as a function of exposure time.
- At the longest exposure time reported, that is, 10000 h, several other kinds of crystalline precipitates appear. The precipitates have different contrasts in the corresponding backscattered SEM image.

EDS analysis was performed in all areas of the bead + 8YSZ substrate specimen to determine the chemical composition of the phases. Figure 4 shows a representative elemental map from the middle top portion of an SCN glass specimen that was exposed for 5000 h to steam + H_2 + N_2. This area shows the presence of three types of precipitates: (a) fine elongated precipitates that nucleate homogeneously in the glass matrix and are rich in K and Al. X-ray diffraction identified these precipitates as potassium feldspar ($KAlSi_3O_8$). (b) Another phase that appears light in the backscattered electron (BSE) images which is rich in barium. This phase was identified by XRD

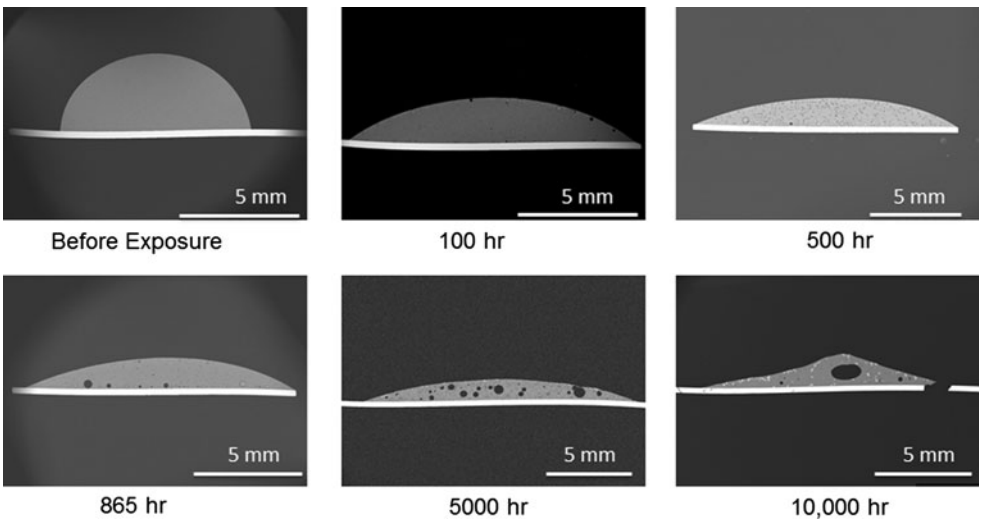

Fig. 2 The effect of exposure to a gas mixture of steam + H_2 + N_2 on the dimensional stability of SCN glass beads on 8YSZ substrate. Glass continues to flow laterally up to 10000 h as a result of gravitational forces

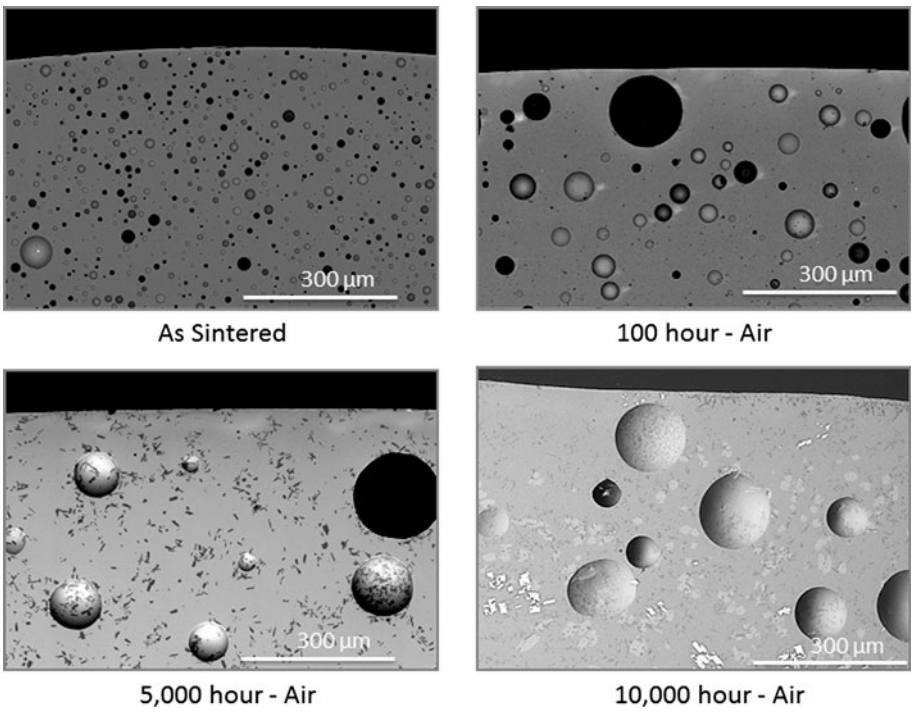

Fig. 3 The effect of long-term air exposure time on the cross-sectional microstructure of SCN glass on 8YSZ substrate

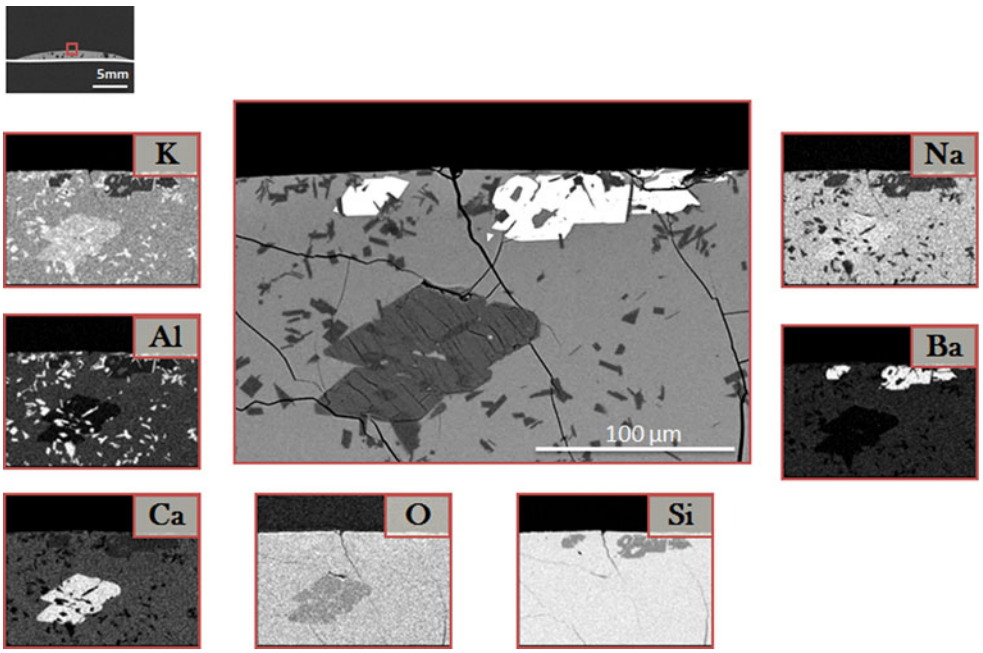

Fig. 4 A representative elemental map (from EDS analysis) from the middle top portion of an SCN glass specimen on 8YSZ substrate that was exposed for 5000 h to steam + H_2 + N_2. The chemical composition of the crystalline phases and remnant glass was determined

to be BaO and nucleates preferentially at the surface before appearing in the bulk after 10000-h exposure. (c) A Ca-rich silicate phase with K and Na is also present in it. This phase could not be identified by XRD due to its low concentration. In addition to these phases, the specimen imaged in Fig. 4 shows that the glass matrix contains a network of interpenetrating cracks. The larger precipitates of the Ca-rich silicate have crystallographic cracks. Figure 5 presents an additional chemical compositional map close to the glass substrate interface for a specimen exposed for 10000 h in steam + H_2 + N_2. The three phases noted above are also observed close to the interface. The SCN glass-8YSZ interface remains sharply defined even after 10000 h of exposure to a gas mixture of

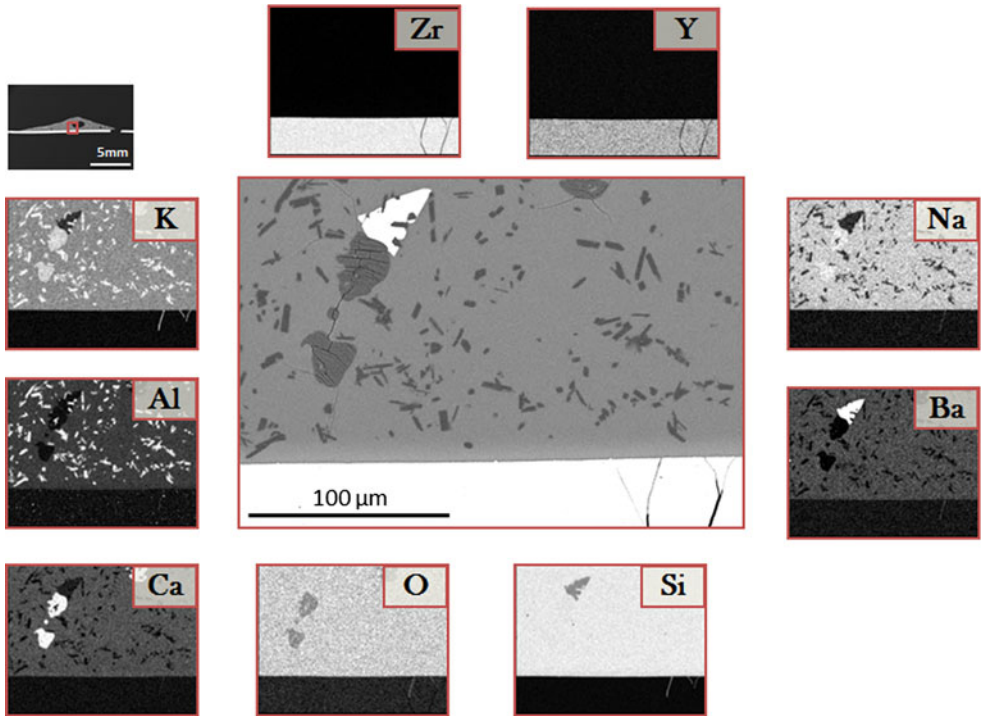

Fig. 5 An elemental map close to the SCN glass/8YSZ substrate interface for a specimen exposed for 10000 h to steam + H_2 + N_2. The interface remains sharp even after long-term exposure

steam + H_2 + N_2, although some cracks appear in the substrate at these longer exposure times. From the elemental maps, it is evident that glass has penetrated the cracks in the 8YSZ substrate.

SCN glass microstructure evolution on alumina substrate

The effects of environment on the microstructural evolution of SCN glass on alumina and 8YSZ were similar. For example, pore coarsening was observed to occur in the glass on alumina as shown for the case of steam + H_2 + N_2 environment in Fig. 6. After 10000 h of exposure, Fig. 6 indicates that nearly all the pores have coalesced into a single large pore suggesting a large driving force for pore coarsening. One observation that holds both for 8YSZ and alumina substrates is that pore coarsening rates are lower in air compared to the steam + H_2 + N_2 environment. This can be concluded by comparing Fig. 7, which shows that the pores in the cross section for 10000 h air-exposed specimens (both 8YSZ and alumina) are not nearly as coarse as those in specimens that were exposed for the same amount of time to the steam + H_2 + N_2 environment (Figs. 2, 6, respectively). The composition and order of appearance of the phases in the air environment are somewhat different from those in the steam + H_2 + N_2 environment. For example, Fig. 8 shows the elemental maps from the top surface of a specimen that was exposed to air for 5000 h. The top surface of the specimen in Fig. 8 shows the presence of crystalline silica with a dendritic structure. The crystalline silica phase was identified as cristobalite by X-ray diffraction. Crystalline silica did not form on the top surface of the glass bead in the case of steam + H_2 + N_2 environment exposure up to 10000 h. The light Ca-rich phase on the top surface also contained Ba in the air environment, and therefore, it had a different chemical composition compared to the corresponding Ca-rich phase that was observed in the steam + H_2 + N_2 environment.

The differences in the type, morphology and order of appearance of crystalline phases in SCN glass between 8YSZ and alumina substrates for both environments were minor. One major physical difference was that the glass beads detached from the alumina substrate at shorter exposure times, whereas they remained attached to the substrate for all conditions for the 8YSZ substrate. This can be concluded by comparing the appearance of the glass-ceramic interface at exposure times of <1000 h in Figs. 2 and 6. At longer exposure times, however, the glass remains attached to the alumina substrate. The onset of glass adhesion to the alumina substrate coincided with the formation of a reaction layer of K-feldspar precipitates close to the glass substrate interface as shown in Fig. 9. A summary of the microstructural evolution in SCN glass with the type and order of appearance of phases is summarized in Table 3a, b for 8YSZ and alumina substrates, respectively.

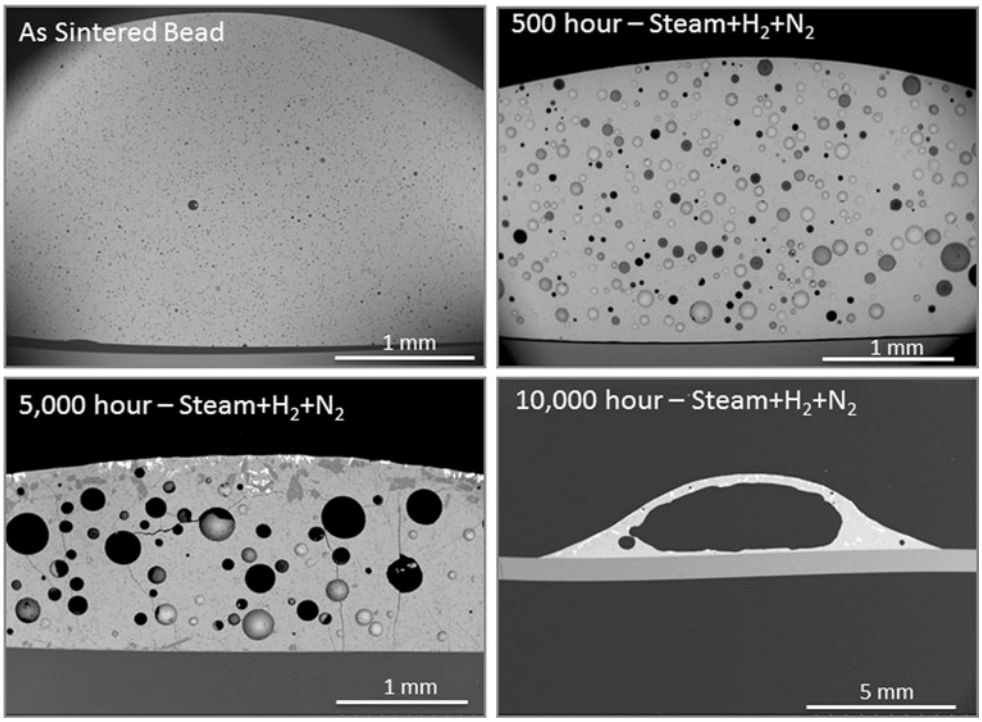

Fig. 6 The effect of steam + H_2 + N_2 environment on the microstructural evolution of SCN glass on alumina substrate. Pore coarsening is readily observed at longer exposure intervals in this figure

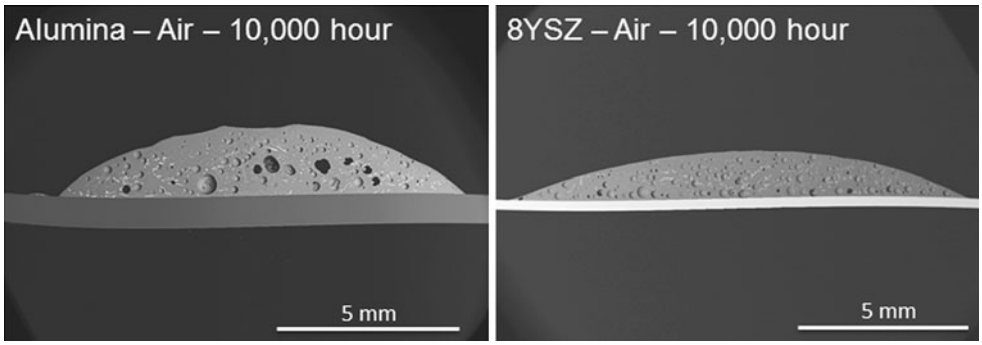

Fig. 7 Pore coarsening is less severe in air environment compared to the steam + H_2 + N_2 environment after 10000-h exposure. The micrographs correspond to alumina (*left*) and 8YSZ substrates and can be compared with corresponding images in Figs. 6 and 2, respectively

SCN glass X-ray diffraction and HRTEM examination

The effect of steam + H_2 + N_2 environment exposure on the evolution of the relative concentration of crystalline phases is illustrated with powder XRD profiles of pulverized glass bead specimens in Fig. 10. The example shown in Fig. 10 is for SCN glass on 8YSZ substrate, but similar analyses were performed for glass on alumina substrate and/or exposed in air. The X-ray diffraction profiles were utilized to identify the fine crystalline phase as $KAlSi_3O_8$. BaO phase was also identified by XRD for specimens exposed to the steam + H_2 + N_2 environments.

A TEM image of a specimen extracted from the interface of SCN glass/8YSZ interface after 850 h of exposure in air is shown in Fig. 11. A thin reaction layer is revealed at the interface in this specimen at this higher magnification. The reaction layer phase was found to be rich in Na, Ba and Ca by EDS analysis.

Quantification of porosity changes with exposure in SCN glass

As was noted in section "SCN glass microstructure evolution on 8YSZ substrate", the average pore size in the glass bead increases with time of exposure. This effect was quantified and a procedure for the determination of porosity and pore size distribution in SCN glass has been reported elsewhere [13]. The effect of time of exposure on the pore size distribution in SCN glass on 8YSZ substrate is summarized in the form of frequency plots in Fig. 12a, b

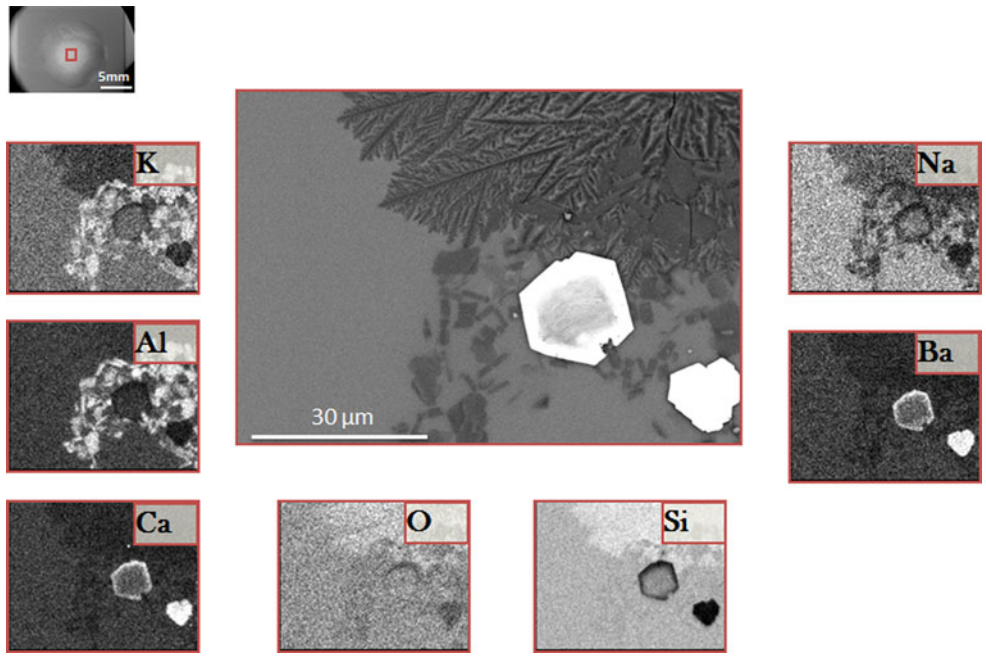

Fig. 8 The elemental maps from the top surface of a specimen that was exposed to air for 5000 h on alumina substrate

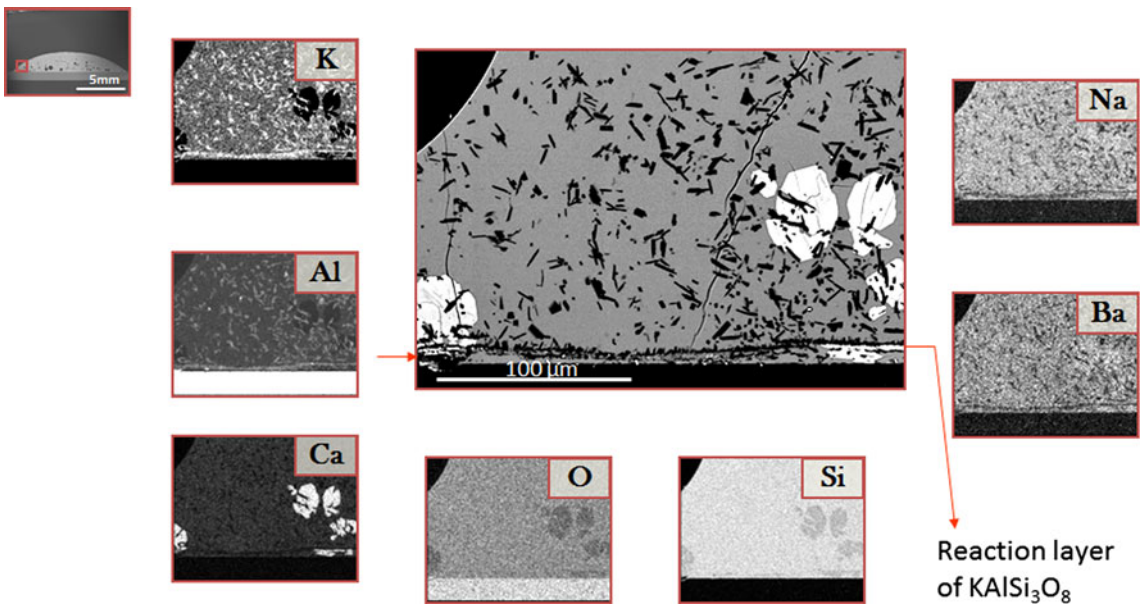

Fig. 9 An elemental map close to the SCN glass/alumina substrate interface for a specimen exposed for 5000 h to air. Glass adhesion to the alumina substrate coincided with the formation of a reaction layer of $KAlSi_3O_8$ precipitates close to the glass substrate interface (Table 3b)

for air and steam + H_2 + N_2 environments, respectively. These results indicate that for both environments, the number of pores decreases and their average size increases as a function of time of exposure. Figure 13, however, shows that the total porosity in the glass bead varies between 10 and 22 % with exposure. The results in Fig. 13 indicate that pore coarsening occurs in SCN glass where the bigger pores may grow at the expense of smaller pores. The extreme example of this is the SCN glass bead on 8YSZ substrate (Fig. 2) that was exposed to the steam + H_2 + N_2 environment for 10000 h where <10 pores remain in the cross section compared to tens of thousands in the as-sintered bead.

The glass cross-sectional area also continues to change with exposure time. For example, for the cross-sectional images in Fig. 2 (8YSZ substrate in steam + H_2 + N_2 environment), the area of the cross section decreases from 19.98 mm^2 for the as-sintered specimen to 14.17 mm^2 for

Table 3 (a) Summary of microstructural evolution for SCN glass on 8YSZ substrate. (b) Summary of microstructural evolution for SCN glass on alumina substrate

Exposure condition	Glass	$KAlSi_3O_8$	Barium type oxide	Ca-rich silicate	SiO_2	Bead attached
(a)						
SCN glass—as-sintered	✔	×	×	×	×	✔
100 h—air	✔	✔	×	×	×	✔
100 h—steam + H_2 + N_2	✔	✔	✔(S)	×	×	✔
500 h—air	✔	✔	×	×	×	✔
500 h—steam + H_2 + N_2	✔	✔	✔(S)	×	×	✔
865 h—air	✔	✔	✔(S)	×	×	✔
850 h—steam + H_2 + N_2	✔	✔	✔(S)	✔(S)	×	✔
5000 h—Air	✔	✔	✔(S)	✔	✔(S)	✔
5000 h—steam + H_2 + N_2	✔	✔	✔(S)	✔	×	✔
10000 h—air	✔	✔	✔	✔	✔(S)	✔
10000 h—steam + H_2 + N_2	✔	✔	✔	✔	×	✔
(b)						
SCN glass—as-sintered	✔	×	×	×	×	×
100 h—air	✔	✔	×	×	×	×
100 h—steam + H_2 + N_2	✔	✔	✔(S)	×	×	×
500 h—air	✔	✔	×	×	×	×
500 h—steam + H_2 + N_2	✔	✔	✔(S)	×	×	×
865 h—air	✔	✔	✔(S)	×	×	✔(r)
850 h—steam + H_2 + N_2	✔	✔	✔(S)	✔(S)	×	×
5000 h—Air	✔	✔	✔(S)	✔	✔(S)	✔(r)
5000 h—steam + H_2 + N_2	✔	✔	✔(S)	✔(S)	×	✔(r)
10000 h—air	✔	✔	✔	✔	✔(S)	✔(r)
10000 h—steam + H_2 + N_2	✔	✔	✔(S)	✔(S)	×	✔(r)

✔(S)—Phase forms only on the surface of the bead

✔(r)—Bead remains attached due to formation of reaction layer

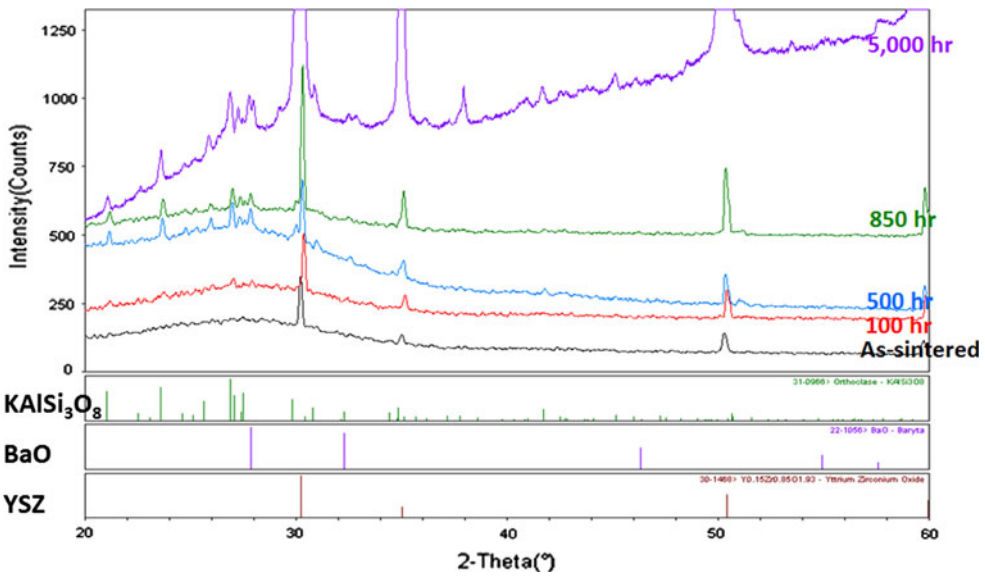

Fig. 10 Example powder XRD profiles of pulverized glass bead specimens that show the effect of steam + H_2 + N_2 environment exposure on the evolution of the relative concentration of crystalline phases for SCN glass on 8YSZ substrate. Similar analysis was performed for glass on alumina substrate and/or in air

5000 h exposure and to 10.43 mm^2 for 10000 h exposure. Since the glass mass change with exposure is small (section "Quantification of porosity changes with exposure in SCN glass") and assuming symmetry in three dimensions, the changes in the cross-sectional area suggest a decrease in the total pore volume with exposure time since the total

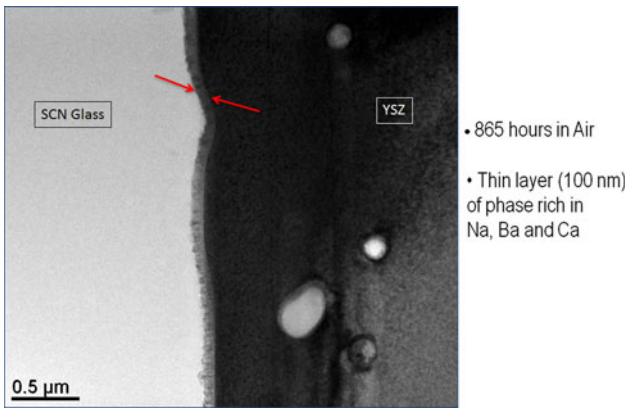

Fig. 11 An HRTEM image of a specimen extracted from the interfacial region of SCN glass/8YSZ substrate after 850 h of exposure in air. A thin reaction layer could be identified at this higher magnification

percentage porosity remains similar or decreases with exposure time (Fig. 13).

SCN glass volatility

Another measurement that was performed on the glass for different exposure times was the mass change. The mass change results for SCN glass on 8YSZ substrate in air and steam + H_2 + N_2 environments are presented in Table 4. The mass change values in Table 4 include the change in mass of the glass bead + substrate system and not the bead alone. Mass change per unit area calculations revealed an anomalously low mass change value at the 5000-h exposure condition. A plot of mass change per unit area was found to be proportional to the square root of time for SCN glass suggesting a diffusion-controlled mechanism for loss of species. For example, the slope of this straight line was ~ -0.04 mg/cm^{2}h$^{0.5}$ in the steam + H_2 + N_2 environment which is comparable to other sealing glasses (for times <1000 h) [14]. The mass change for SCN glass is greater in an air environment compared to the flowing steam + H_2 + N_2 environment. It is noted that the total mass change in SCN glass due to exposure is less in magnitude than −0.76 % under all conditions.

G6 glass microstructural evolution

G6 glass microstructure evolution on 8YSZ substrate

The effect of exposure to the steam + H_2 + N_2 environment on the evolution of the microstructure of G6 glass is illustrated in SEM cross sections in Fig. 14. Images from top to bottom represent the cross section at increasing magnifications, whereas from the left to right the images represent longer exposure times. The total porosity and fraction of crystalline phases in G6 glass is lower than those for SCN glass for all exposure levels. Pore coarsening along with pore migration to the top free surface were observed at longer exposure times in the steam-containing environment. It is noted that the crystalline phases that formed at longer exposure times in the steam + H_2 + N_2 environment were also concentrated closer to the top free surface of the bead.

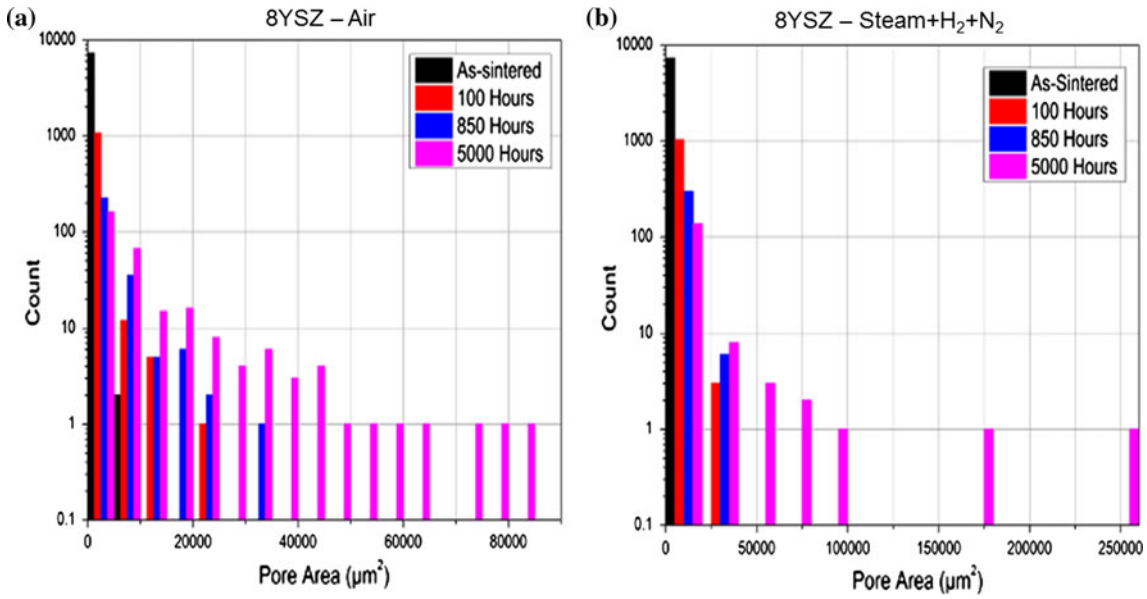

Fig. 12 The effect of time of exposure on the pore size distribution in SCN glass on 8YSZ substrate in **a** air and **b** steam + H_2 + N_2 environment. In all exposure conditions, the number of pores decrease and their average size increase at longer times of exposure

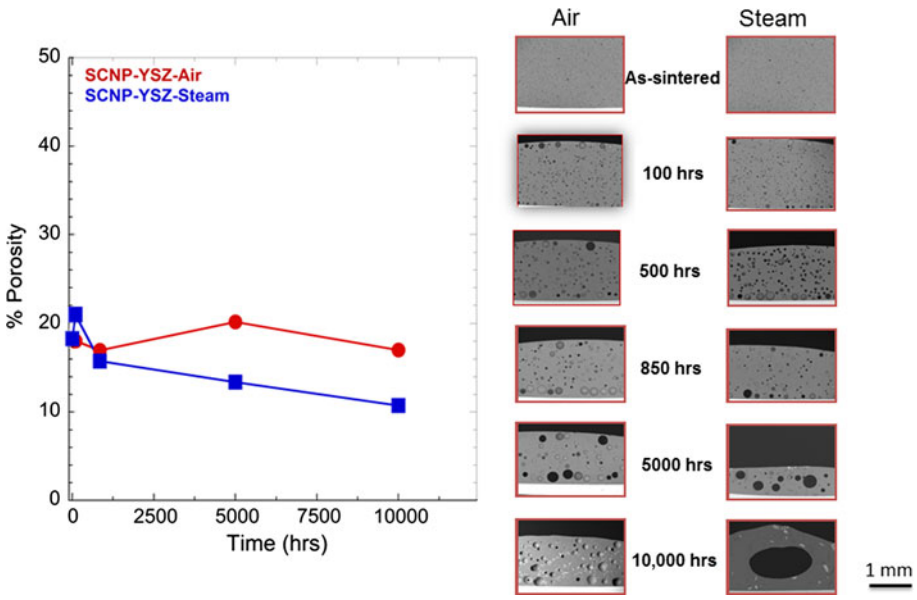

Fig. 13 The total porosity in SCN glass beads as a function of exposure time for air and steam + H_2 + N_2 environments on 8YSZ substrate. Representative micrographs for individual exposure conditions are included in this figure

Table 4 Weight change in exposure specimens under different conditions. Data for SCN and G6 glasses in air and steam + H_2 + N_2 environment on alumina and 8YSZ substrates are included

Glass	Substrate	Exposure environment	Exposure time	Weight change (%)
SCN	Alumina	Steam + H_2 + N_2	100 h	−0.05
SCN	Alumina	Steam + H_2 + N_2	500 h	−0.12
SCN	Alumina	Steam + H_2 + N_2	5000 h	−0.04
SCN	Alumina	Steam + H_2 + N_2	10000 h	−0.27
SCN	Alumina	Air	100 h	−0.12
SCN	Alumina	Air	500 h	−0.43
SCN	Alumina	Air	5000 h	−0.09
SCN	Alumina	Air	10000 h	−0.70
SCN	8YSZ	Steam + H_2 + N_2	100 h	−0.11
SCN	8YSZ	Steam + H_2 + N_2	500 h	−0.21
SCN	8YSZ	Steam + H_2 + N_2	5000 h	−0.09
SCN	8YSZ	Air	100 h	−0.26
SCN	8YSZ	Air	500 h	−0.62
SCN	8YSZ	Air	5000 h	−0.11
SCN	8YSZ	Air	10000 h	−0.76
G6	Alumina	Steam + H_2 + N_2	100 h	−0.04
G6	Alumina	Steam + H_2 + N_2	500 h	−0.09
G6	Alumina	Steam + H_2 + N_2	5000 h	−0.14
G6	Alumina	Steam + H_2 + N_2	10000 h	−0.21
G6	Alumina	Air	100 h	−0.04
G6	Alumina	Air	500 h	−0.16
G6	Alumina	Air	10000 h	−0.18
G6	8YSZ	Steam + H_2 + N_2	100 h	−0.05
G6	8YSZ	Steam + H_2 + N_2	500 h	−0.17
G6	8YSZ	Steam + H_2 + N_2	10000 h	−0.34
G6	8YSZ	Air	100 h	−0.04
G6	8YSZ	Air	500 h	−0.21
G6	8YSZ	Air	5000 h	−0.43
G6	8YSZ	Air	10000 h	−0.54

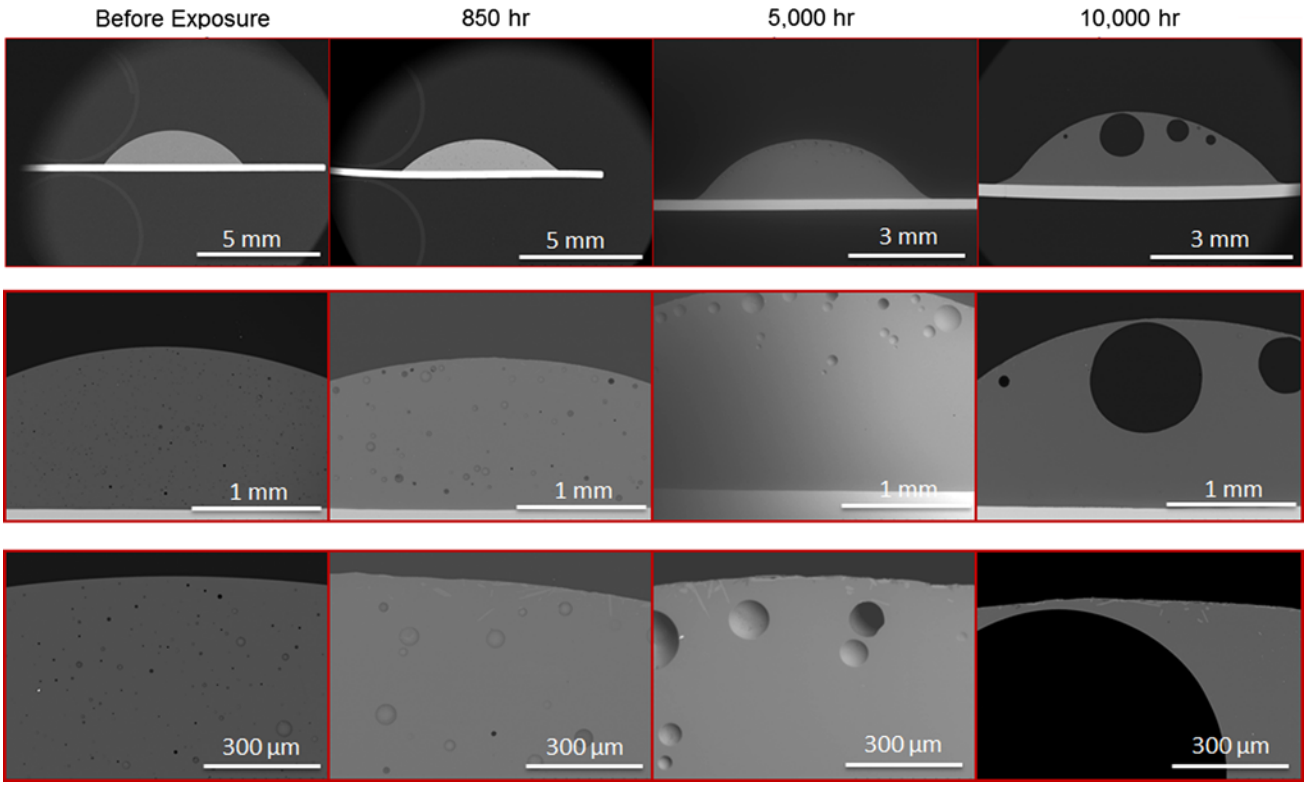

Fig. 14 The effect of exposure to steam + H_2 + N_2 environment on microstructural evolution in G6 glass on 8YSZ substrate. The cross-sectional micrographs indicate a pore migration phenomenon in addition to the pore coarsening observed for SCN glass

The results for G6 glass in the steam + H_2 + N_2 environment are qualitatively comparable for exposure in air environment and are summarized via Fig. 15. For example, pore coarsening is observed, but the pore migration observed in the steam + H_2 + N_2 environment is not as obvious in the air environment (compare Figs. 14, 15). This coincides with the crystalline phases distributed relatively homogenously throughout the cross section in the air-exposed specimens shown in Fig. 15. Since the crystallization resistance of G6 glass is better than that of SCN glass, the microstructure of G6 glass evolves at a slower pace. In addition, the initial porosity in G6 glass is lower compared to SCN glass. We will, therefore, discuss microstructural changes in G6 glass for the longest time exposure, that is, 10000 h in air and the steam + H_2 + N_2 environment, for either alumina or 8YSZ substrates.

G6 glass microstructure after 10000-h exposure

Evolution of the microstructure in G6 glass after 10000 h of exposure is summarized in Fig. 16. Micrographs of G6 glass beads exposed to both air and steam + H_2 + N_2 environments on alumina and 8YSZ substrates are shown in this figure. The better crystallization resistance of G6 glass in comparison with that of SCN glass is evident in Fig. 16 as indicated by the low volume percentage of crystalline phases formed in the glass even after very long-term exposure. In addition, even though pore coarsening has occurred, the total porosity remains low in air and gets accumulated into a few large pores for the steam + H_2 + N_2 exposure environment. Another observation about the pores in G6 glass after 10000 h of exposure is that they are homogenously distributed in samples exposed to air, but they migrate toward the top surface of the bead in the steam + H_2 + N_2 environment after very long exposure times.

While the glass maintains a geometrically well-defined bead shape on 8YSZ substrate, as shown in Fig. 16, glass beads on alumina substrate were distorted due to the formation of a surface crust layer of crystalline precipitates. In addition to fewer pores and crystalline precipitates, G6 glass specimens also had a lower density of cracks compared to SCN specimens at similar levels of exposure. Compared to SCN glass, the reaction between the G6 glass and 8YSZ substrate was more evident in the case of 8YSZ substrate and also a reaction layer formed between G6 glass and alumina substrate as can be seen in the bright regions in Fig. 16 (see arrows). TEM characterization of the interfacial region between G6 glass and 8YSZ substrate after 10000 h of steam + H_2 + N_2 exposure is summarized in Fig. 17. A multilayer reaction region formed between the glass and the 8YSZ substrate with a compound of the composition Na–Si–Ca–Zr–O (with thickness over

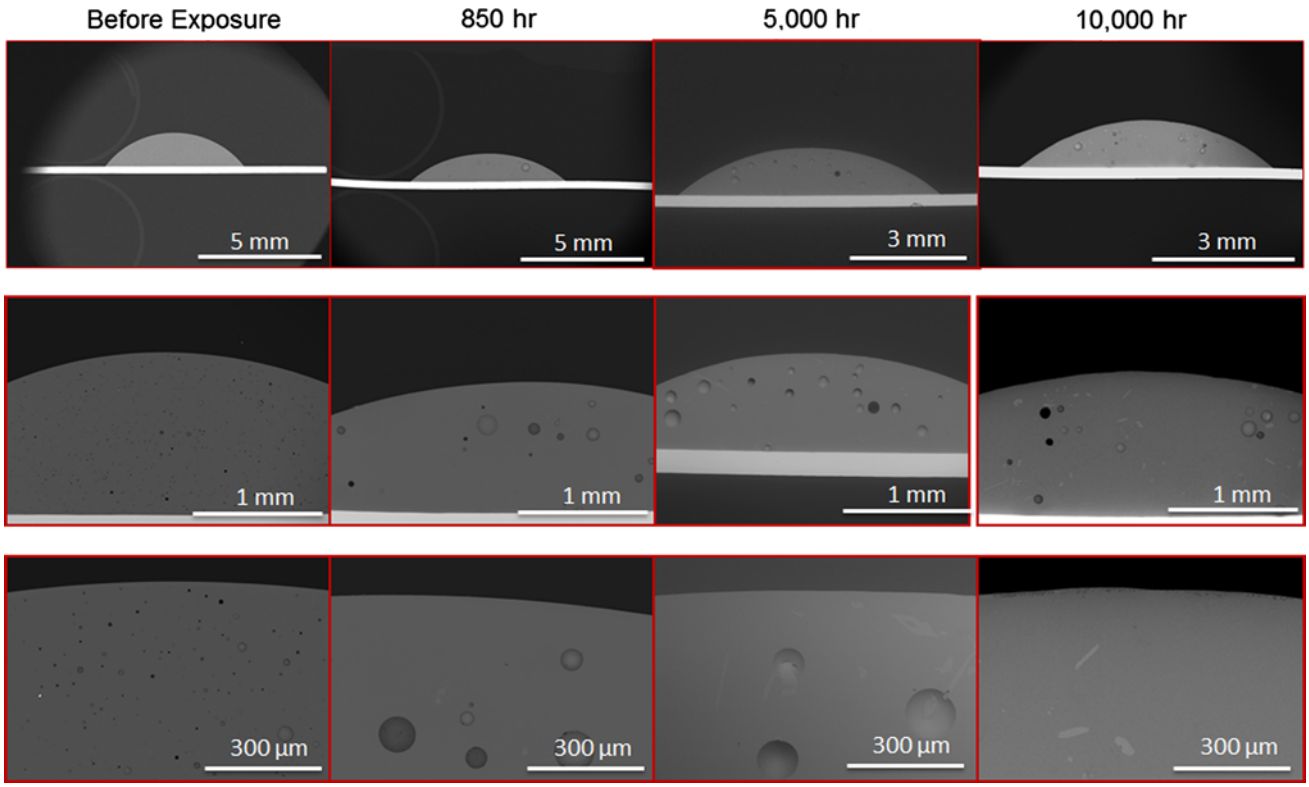

Fig. 15 The effect of exposure to air environment on microstructural evolution in G6 glass on 8YSZ substrate

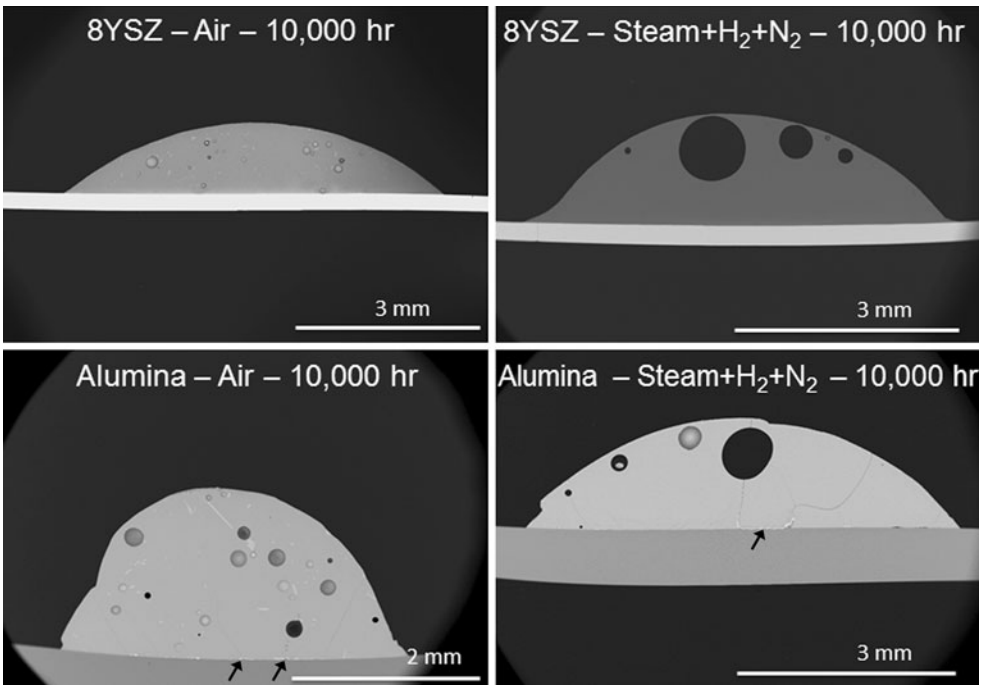

Fig. 16 A summary of the microstructural evolution in G6 glass after 10000 h of exposure. The exposure conditions are noted in the micrographs

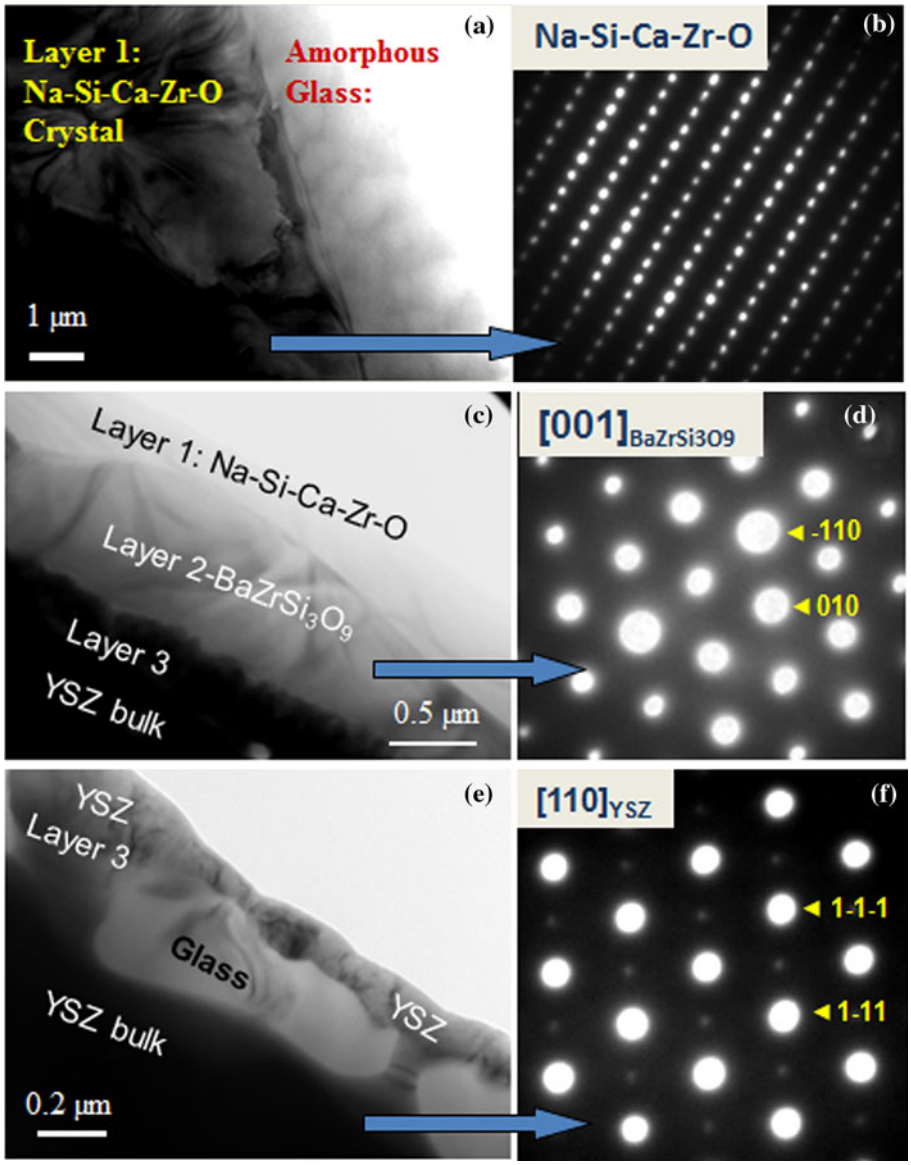

Fig. 17 A summary of HRTEM characterization of the interfacial region of G6 glass/8YSZ substrate after 10000 h of steam + H_2 + N_2 exposure. A multilayer reaction region formed between glass and the substrate. **a**, **b** show the morphology and electron diffraction from the crystalline Na–Si–Ca–Zr–O layer which is underneath the amorphous glass; **c**, **d** show the morphology and the electron diffraction of the $BaZrSi_3O_9$ crystals that are close to the YSZ substrate; **e**, **f** show the morphology and the electron diffraction from the interface of $BaZrSi_3O_9$ and YSZ substrate. Some amorphous glass particulates penetrate into the YSZ grains

1 μm) on the glass side and $BaZrSi_3O_9$ (with thickness over 1 μm) on the substrate side. The interlocking nature of the microstructure of the reaction layers suggests that the layers provide good mechanical adherence between the glass and the substrate.

X-ray diffraction of air-exposed specimens detected no crystallization in G6 glass up to 5000 h for the 8YSZ substrate samples and up to 850 h for the alumina substrate specimens. After 10000 h of exposure, diopside ($MgCaSi_2O_6$) and wollastonite ($CaSiO_3$) appear in air-exposed specimens on both substrates. The presence of magnesium- and calcium-rich silicates in the G6 glass microstructure was confirmed by EDS mapping of the specimen cross sections.

Porosity changes with exposure in G6 glass

The changes in the total porosity of G6 glass on 8YSZ substrate as a function of exposure time are shown in Fig. 18. The total porosity in G6 glass is smaller compared to SCN glass as can be seen by comparing the results in Fig. 18 with Fig. 13. Pore coarsening occurred in G6 glass as well where the average size of the pores increased with time. In one condition, namely steam + H_2 + N_2 exposure for 10000 h, however, the total porosity in the glass increased compared to corresponding shorter exposure intervals. In other conditions analyzed, the total area fraction of porosity in the glass bead remained in the 3–4 % range.

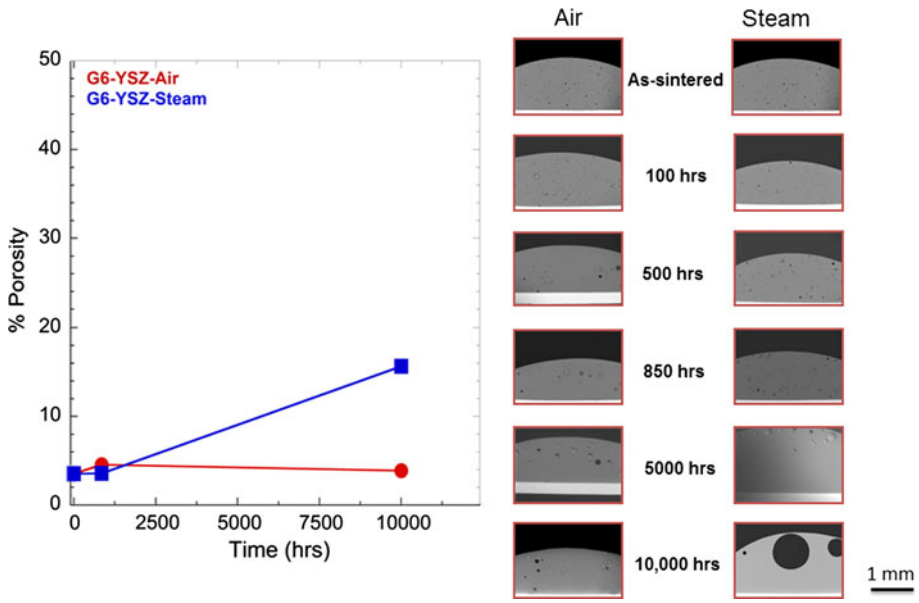

Fig. 18 The total porosity in G6 glass beads as a function of exposure time for air and steam + H_2 + N_2 environments on 8YSZ substrate. The total porosity in G6 glass specimens is lower compared to SCN glass (compare this figure with Fig. 14)

G6 glass volatility

The mass change results for G6 glass on 8YSZ substrate in air and steam + H_2 + N_2 environments are also included in Table 4. The mass change per unit time per unit area in G6 glass is less (in magnitude) than −0.54 % under all conditions. The average mass change in G6 glass for all exposure conditions listed in Table 4 is −0.19 %, which is better than the average mass change for SCN glass of −0.27 %.

Discussion

Chemical composition differences between SCN and G6 glass and implications for thermal properties

The chemical compositions of SCN and G6 glass in oxide mol% are listed in Table 1. The main components of glasses considered for SOFC sealing applications are network formers, network modifiers, intermediate oxides and minor additives [5]. The common glass network formers are SiO_2 and B_2O_3. SCN glass contains SiO_2 alone as glass former, but G6 glass contains B_2O_3 in addition to SiO_2. The major constituents of the two glasses analyzed, apart from the network formers, are the network modifiers. SCN glass has a higher total concentration of network modifier oxides (K_2O, Na_2O, BaO, CaO and MgO) totaling 23.5 mol%, whereas the total concentration for these oxides is 19.0 mol% in G6 glass. In addition, SCN glass has a higher total alkali oxide (K_2O and Na_2O) content of 13.3 mol% compared to 10.4 mol% for G6 glass. The difference in the concentration of network modifiers has consequences on the thermomechanical and functional properties of these glasses. Both glasses have Al_2O_3 in the 2–3 mol% concentration range, and alumina serves as an intermediate oxide that can act either as a network former or as a modifier. TiO_2 is present in SCN at 0.5 mol% and ZnO is present in G6 at 3.0 mol%, and they are additives that influence devitrification of the glasses.

The effect of compositional differences outlined above on the thermal properties of the glasses is discussed below. It is well known that replacement of SiO_2 by B_2O_3 leads to a decrease in T_g and an increase in the CTE of the glass [5, 15, 16]. Since G6 glass with 9.5 mol% B_2O_3 as a network former has a lower CTE compared to SCN by about 2×10^{-6} °C^{-1} [10] and also has somewhat higher T_g values [10], it is concluded that the thermal behavior of the glasses are not dictated by the network formers. The concentration of network modifiers has a more significant bearing on determining the thermal properties of sealing glasses [5]. Since SCN glass has a higher concentration of network modifiers compared with G6, its higher CTE and lower T_g are consistent with the above explanation.

Thermochemical stability and devitrification of SCN and G6 glasses

Although devitrification resistance and thermochemical stability are prime requirements for SOFC glass seal materials, they are not well understood for multicomponent glasses [4, 5]. In general, reported trends for devitrification resistance are the following: (1) increasing silica content (compared to B_2O_3) as a glass former increases devitrification resistance

[17]; (2) network modifiers with increasing field strength increase the devitrification resistance in the following order (Mg > Ca > Ba) [18]; (3) intermediate oxides like alumina hinder phase separation [19]; and (4) additives generally reduce the devitrification resistance in sealing glasses. Of the major oxide constituents in SCN and G6 glass shown in Table 1, it was shown that a reduction in the concentration of BaO increases the devitrification resistance of SiO_2–B_2O_3–BaO glasses [20]. The last observation holds when comparing SCN and G6 glasses since the latter has lower BaO content and higher devitrification resistance. Other trends summarized above are in conflict with experimental observations such as G6 glass has much higher B_2O_3 and additive (3 mol% ZnO compared to 0.5 mol% TiO_2 in SCN) content, which should both otherwise promote devitrification. The experimental observations suggest that general trends observed for two or three component glasses may not be applicable for the two multicomponent glasses investigated in this study.

A physical property that correlates with phase separation and devitrification is the viscosity of the glass [21] with higher viscosity promoting devitrification resistance. This may be expected since viscosity plays an important role in determining the mass transport in melts. For example, addition of alkali oxide dramatically decreases the viscosity of the glass by decreasing the connectivity of the structure and that in turn promotes phase separation. The viscosity of G6 is lower compared to SCN glass below 700 °C, but between 700 and 800 °C, the viscosity values for the two glasses are comparable [10]. In addition, lower-viscosity glasses also have higher reactivity since liquids are more reactive compared to solids. Since the viscosity value of the two glasses is comparable at 800 °C, none of the differences in devitrification resistance and chemical reactivity could be attributed to viscosity differences between the glasses.

Comparison of the microstructure evolution of SCN and G6 glasses

The following pore distribution evolution trends are summarized below for discussions to follow:

- Porosity is finely distributed in the glasses in the as-sintered state. Exposure to both environments leads to coarsening of pores so that the mean pore size increases (Figs. 2, 6, 14, 15).
- Pore coarsening is faster in steam + H_2 + N_2 compared to air exposure environment (compare Figs. 6, 7 for SCN and 16 for G6).
- Pore coarsening rates are higher for glasses on alumina substrate compared to 8YSZ substrate (Fig. 7 for SCN glass comparison and 16 for G6 glass comparison).
- While porosity is homogeneously distributed in the case of SCN glass (Fig. 6, 7), the pores tend to migrate to the top surface in the case of G6 glass (Fig. 14, 15, 16). The occurrence of pore migration is obvious in the specimens exposed to the steam + H_2 + N_2 environment.

The coarsening of pores in a viscous solid has been modeled by Scherer [22] who attributed pore coarsening to the constraints imposed on the viscous solid. The coarsening rate according to the Scherer model is proportional to γ/η, where γ is the viscous solid–vapor interfacial energy and η is the viscosity. The viscosity and the wetting characteristics of SCN and G6 glasses are comparable at 800 °C, [10] so the two materials should have comparable pore coarsening rates. There is evidence that glass flows at a higher rate in the steam + H_2 + N_2 environment compared to air as shown by the lower dynamic contact angle in the moisture containing environment (Fig. 19). Other researchers have attributed the higher wetting of glass in steam to the increase in non-bridging oxygen and electronegativity of the glass surface in the presence of steam [23]. The lower viscosity of the glass in steam can help explain the higher pore coarsening rates. Also, due to a greater CTE mismatch, the constraints in the glass will be higher for exposure on the alumina substrate compared to 8YSZ substrate. Although constraint effects are diminished above T_g, constraint effects along with surface tension (alumina specimens have higher dynamic contact angles compared to 8YSZ specimens and therefore a higher interfacial energy) changes may explain the higher coarsening rate of the glasses on alumina compared to 8YSZ. Finally, there are two sources of constraint in the material: the substrate and the harder crystalline phases. In the case of SCN, the homogeneous distribution of crystalline

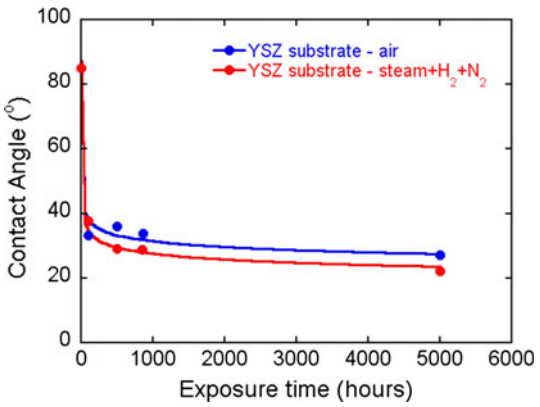

Fig. 19 Effect of exposure time on the dynamic contact angle between SCN glass and 8YSZ substrate. The contact angles are lower in the steam + H_2 + N_2 environment compared to the air environment

precipitates likely promotes homogenous pore coarsening in that glass. In G6 glass, however, the surface crystallization in the steam-rich environment may provide an additional local driving force for pore coarsening and that may explain the pore migration phenomenon noted above.

The following microstructural evolution trends and features are summarized below for discussions to follow:

- While some phases nucleate homogeneously in the bulk ($KAlSi_3O_8$ in SCN), others nucleate on the surface (e.g., BaO in SCN) and then in the bulk after prolonged exposure (see Table 3 for detailed comparison for SCN glass).
- The type and order of appearance of the phases are similar for the two environments and for both substrates.
- A reaction layer forms between the glass and the substrate after prolonged exposure. In the case of alumina, this reaction layer consists of $KAlSi_3O_8$. In the case of 8YSZ and SCN glass, the reaction layer is continuous and much thinner and therefore can only be observed by TEM (Fig. 11).
- Crystallization in the glass leads to the development of cracks likely formed during cooling of the specimen from exposure temperature. For SCN glass, the cracks develop into extended networks in the glass as shown in Fig. 4. The crack density in G6 glass is much lower and appears only after extended times of exposure as shown in Fig. 16.

The heterogeneous nucleation of certain phases on the surface (e.g., BaO in SCN glass) followed by their homogeneous nucleation suggests that phase separation continues to occur at longer exposure times in the glass. The complex nature of multicomponent glasses makes it difficult to make accurate thermodynamic and kinetic predictions of the nature and volume fraction of crystalline phases. An experimental study such as the present one is necessary to document the extent of crystallization. In general, the distribution of crystalline phases formed is a weaker function of environment and substrate type compared to the pore size distribution. The crystalline phases formed are obviously different for G6 and SCN glasses consistent with the differences in their composition. G6 glass has much higher devitrification resistance compared to SCN glass as discussed earlier.

An important difference between the results of environmental exposure of the glasses on different substrates is the nature and size of the interfacial/reaction layer. For example, the reaction layer of orthoclase ($KAlSi_3O_8$) precipitates lets the bead stay attached to the alumina substrate as shown in Fig. 9 by lowering the local CTE of the glass and reducing the CTE mismatch in thermal expansion with the substrate. Orthoclase has a density of 2.57 g/cc [24], which is close to the density of SCN glass of 2.49 g/cc [10]. The CTE of orthoclase, however, is 5.2×10^{-6} °C^{-1} between 20 and 500 °C [24], which is significantly lower than that of SCN glass which has a CTE of 12.9×10^{-6} °C^{-1} between 20 and 400 °C [10]. However, the average of the CTE values of SCN glass and orthoclase is close to the CTE of alumina, which is in the $8.7–9.0 \times 10^{-6}$ °C^{-1} range. In the absence of the reaction layer, that is, at shorter exposure times, the glass detaches from the alumina substrate as noted in Table 3b. In addition, the dimensional changes associated with the crystallization can themselves lead to a lowering of interfacial stress. A plausible explanation for the formation of K-feldspar-rich reaction layer is the availability of aluminum ions on the other side of the interface in the case of alumina substrate. While the reaction layer in the case of 8YSZ is much thinner (Fig. 11), it nevertheless will be expected to play an important role in the thermal stress development and durability of the glass seal. Finally, devitrification generally leads to a crystalline phase(s) with lower CTE than the precursor glass [5] and the latter promote the development of stresses during cooling below the glass transition temperature that lead to crack formation (for example see Fig. 4 for SCN glass and Fig. 16 for G6 glass). It is worth noting that microcracking in the complex silicate phases (Figs. 4, 5) will further lower the overall CTE of the glass since the microcracks form perpendicular to higher CTE directions in the crystal lattice [25]. Furthermore, crystalline phases with alkali and alkaline earth ions will reduce the CTE of the glass matrix itself since these ions are responsible for increasing the CTE of these glasses. The crack density in the glasses increases with increasing devitrification at longer exposure times. G6 glass has a significantly lower crack density consistent with its higher devitrification resistance even though the CTE mismatch between G6 and 8YSZ substrate is expected to be greater compared to SCN glass.

Microstructure evolution and its effect on thermophysical properties

Since the glasses discussed in the present investigation could be potentially used for SOFC sealing applications, the effect of microstructural evolution on the thermal stress development in seals is discussed in this section. As a first approximation, the thermal stresses (σ_t) in the glass seal can be estimated [9, 26] by applying the following relationship, $\sigma_t = \Delta\alpha\Delta TE$, where $\Delta\alpha$ is the difference in CTE between the glass and the substrate, ΔT is difference between the temperature and the glass transition temperature, and E is the Young's modulus of the glass. With the evolution of microstructure, the three properties that determine the thermal stresses in the seal will also evolve.

In general, the overall CTE decreases with the formation of crystalline phases [5] as the increase in CTE due to crystallization has been observed only in rare cases [20]. The decrease in CTE with respect to the initial CTE which is tailored to match the CTE of adjacent SOFC components will increase the stresses that form in the seal. A change in the pore size distribution or total porosity is not expected to change the CTE of the seal. SCN glass has a higher CTE of $\sim 12 \times 10^{-6}$ °C^{-1} compared to $\sim 10 \times 10^{-6}$ °C^{-1} for [10] G6 glass at 400 °C. Since crystalline phases lower the overall CTE of the material, the lower initial CTE in G6 glass may be compensated by its higher devitrification resistance compared to SCN glass. The glass transition temperature of the two exposed glasses remains nearly unchanged due to prolonged exposure (unpublished results). This behavior indicates that the glass retains its underlying network structure and a change in T_g does not contribute to the change in thermal stress development as a function of exposure time. The contribution in thermal stresses at lower temperatures due to T_g will be marginally higher for G6 glass since the T_g value for this glass is higher than that of SCN glass by ~ 50 °C [10]. The mass change results in Table 4 indicate that the loss of alkali elements from the glasses due to vaporization is not substantial, and this may explain the insensitivity of T_g to prolonged exposure in the two environments.

It has been reported that the Young's modulus of SCN glass in the as-sintered state is 52 GPa at room temperature and lower than the corresponding value for G6 glass of 72 GPa [10]. This difference is related to higher initial porosity in SCN glass which is of the order of 20 volume % compared to <5 % for G6 glass. The primary manner by which the porosity can influence the behavior of the glass seal will be via the extreme constituents of the pore size distribution, that is, the largest pores in Fig. 12. The largest pores will cause heterogeneity of properties, and in the worst case, a rupture of the area around them that will compromise the integrity of the entire seal.

Projection of microstructure for individual phases and porosity

It is noted that the current experimental approach of exposing a glass bead in a particular (air/steam + H_2 + N_2) environment presents a worst-case scenario where a large surface area of the bead is exposed to the environment. In large SOFC stacks, the seal material may be applied as a thin layer on a coated interconnect and is exposed to a dual environment on opposite sides of the seal simultaneously.

An advantage of an experimental evaluation of the microstructural evolution is that the predictions for microstructure and property extrapolations can be further refined. For example, the volume fraction of the $KAlSi_3O_8$ phase in SCN glass increases with increasing exposure time. While the time dependence of the volume fraction increase follows the classical Johnson–Mehl–Avrami (JMA) kinetics in the shorter exposure times (<5000 h), at extended exposure times, deviations from the JMA behavior is observed. This behavior is similar to the crystallization behavior of other phases reported in glass seal systems as summarized by Mahapatra and Lu [5]. There are several reasons for deviation from JMA kinetics including the heterogeneous nature of nucleation sites and in the case of SCN glass, the possible exhaustion of potassium and aluminum from the glass matrix at longer exposure times.

The evolution of the porosity reported in the present study and in particular the pore coarsening has not been reported previously in a systematic manner. Models for describing the pore coarsening behavior are being implemented currently and will be reported in the near future. These models will allow the prediction of the time elapsed before the porosity will collapse into a single unit. Since SOFCs are expected to operate for 40000 h with acceptable levels of degradation, such predictive capability will be valuable for long-term performance of these devices.

Conclusions

The very long-term microstructural and chemical stabilities of two glasses with potential for use in SOFC sealing applications, namely SCN and G6, were experimentally determined. The multicomponent glasses were exposed to air or to a gas mixture of steam + H_2 + N_2 on alumina or 8YSZ substrates for up to 10000 h. It was observed that these multicomponent glasses followed few rules for chemical and microstructural stability reported in the literature. Furthermore, it was found that the glasses had adequate devitrification resistance with G6 glass having superior resistance compared to SCN. Pore coarsening occurs in the glasses where the larger pores grow at the expense of smaller pores, and this phenomenon was faster in the presence of the steam + H_2 + N_2 environment and/or on the alumina substrate. In the extreme case, the pores coalesced into a single unit that could threaten the integrity of the seal. The trends in pore coarsening were well explained by existing viscous media pore coarsening models. Other than the porosity change concerns, it was concluded that the glasses could provide adequate sealing for long-term operation. Results of the present long-term exposure indicate that designers should take into account the change in properties that accompany microstructural changes after prolonged exposure in order to increase the durability of the SOFC system.

Acknowledgements This research work was sponsored by the US Department of Energy, Office of Fossil Energy, SECA Core Technology Program at ORNL. The authors are grateful for the support of NETL program managers Rin Burke, Wayne Surdoval, Travis Shultz and Shailesh Vora. The authors thank James Hemrick (ORNL) for reviewing the manuscript.

References

1. Ormerod RM (2003) Chem Soc Rev 32:17
2. Nagel FP, Schildhauer TJ, Biollaz SMA, Wokaun A (2008) J Power Sources 184:143
3. Fergus JW (2005) J Power Sources 147:46
4. Mahapatra MK, Lu K (2010) J Power Sources 195:7129
5. Mahapatra MK, Lu K (2010) Mat Sci Eng R 67:65
6. Taniguchi S, Kadowaki M, Yasuo T, Akiyama Y, Miyake Y, Nishio K (2000) J Power Sources 90:163
7. Meinhardt KD, Kim DS, Chou YS, Weil KS (2008) J Power Sources 182:188
8. Singh RN (2007) Int J Appl Ceram Tech 4:134
9. Chou Y-S, Thomsen EC, Williams RT, Choi JP, Canfield NL, Bonnett JF, Stevenson JW, Shyam A, Lara-Curzio E (2011) J Power Sources 196:2709
10. Trejo R, Lara-Curzio E, Shyam A, Kirkham M, Garcia-Negron V, Wang Y (2012) Int J Appl Glass Sci 3:369
11. Chou Y-S, Thomsen EC, Choi JP, Stevenson JW (2012) J Power Sources 197:154
12. Chou Y-S, Choi JP, Stevenson JW (2012) Int J Hyd Energy 37:18372
13. Ladouceur A, Shyam A, Trejo RM, Lara-Curzio E (2013) (to be submitted)
14. Zhang T, Fahrenholtz WG, Reis ST, Brow RK (2008) J Amer Cer Soc 91:2564
15. Mahapatra M, Lu K, Bodnar R (2009) Appl Phys A Mater Sci Process 95:493
16. Sohn S-B, Choi S-Y, Kim G-H, Song H-S, Kim G-D (2004) J Am Ceram Soc 87:254
17. Lara C, Pascual MJ, Durán A (2004) J Non Cryst Solids 348:149
18. Lahl N, Singh K, Singheiser L, Hilpert K, Bahadur D (2000) J Mat Sci 35:3089
19. Mahapatra MK, Lu K, Reynolds WT Jr (2008) J Power Sources 179:106
20. Peng L, Zhu Q (2008) J Fuel Cell Sci Tech 5(3):031210
21. Shelby JE (2005) Introduction to glass science and technology, 2nd edn. Royal Society of Chemistry, Cambridge
22. Scherer GW (1998) J Am Ceram Soc 81:49
23. Simhan RG, Moore LL, Gunten PR (1985) J Mat Sci 20:1748
24. Winkler EM (1975) Stone: properties, durability in man's environment, 2nd edn. Springer, New York
25. Shyam A, Lara-Curzio E, Pandey A, Watkins TR, More KL (2012) J Am Ceram Soc 95:1682
26. Chou Y-S, Stevenson JW (2002) J Power Sources 112:376